ROYAL SOCIETY OF CHEMISTRY

PAPER

Check for updates

A highly sensitive self-powered photodetector based on pinhole-free PEA$_{0.2}$FA$_{0.8}$SnI$_3$ films with aminopyrimidine†

Meiyue Liu, [ID] [a] Yuanchuang Li,[a] Xiang Yao,*[b] Shengjun Li [ID] [a] and Hin-Lap Yip [ID] *[cde]

Tin-based perovskite halides have emerged as promising lead-free perovskite photodetectors. However, achieving high performance is hampered by poor stability and a high density of intrinsic defects. In this study, we developed an efficient tin-based perovskite photodetector that is sensitive to visible and near-infrared light through the incorporation of 2-aminopyrimidine as an additive. Our results demonstrated that the inclusion of 2-aminopyrimidine significantly improves film morphology, reduces roughness, passivates defect states, and suppresses the oxidation of Sn^{2+}. The PEA$_{0.2}$FA$_{0.8}$SnI$_3$ films with 2-aminopyrimidine exhibited a high responsivity of 0.4 A W^{-1} and a detectivity of 1.16 × 10^{12} Jones, a fast response time of 0.93 ms, and excellent operation stability after 10^4 on/off cycles. The findings highlight the significant potential of tin-based perovskite in the development of advanced photodetectors.

Introduction

Photodetectors (PDs) are capable of sensing optical signals over a wide range of wavelengths, including ultraviolet, visible light, and near-infrared (NIR) light. NIR detection is particularly important for various optical–electrical applications, such as medical imaging, biometric identification, and image sensing.[1–3] However, current commercial NIR PDs based on inorganic compounds (silicon and III–V group materials) are costly and require high-temperature and vacuum processes.[4,5] The development of new materials, such as conjugated molecules, two-dimensional materials, and halide perovskites, has led to the creation of lighter and lower-cost PDs.[6–9] Organic–inorganic halide perovskites, in particular, are promising options as next-generation PDs due to their low cost, ease of fabrication, and excellent optoelectronic properties.[10–18] Although Pb-based perovskite PDs have demonstrated high responsivity, detectivity, and fast response time,[19–21] the toxicity of Pb limits their commercialization.[22,23] Substitution of Pb with

a less toxic alternative is therefore necessary to ensure commercial viability.

Tin (Sn)-based perovskites have emerged as a possible solution that addresses the issue of toxicity in Pb-based perovskite PDs, offering the advantages of a narrow bandgap, high charge-carrier mobility, and low exciton binding energy.[24–26] Sn-based perovskites facilitate optical detection ranging from visible to NIR.[27,28] However, most of the previously reported Sn-based PDs are based on nanowire structures, all inorganic perovskites, or 2D perovskites with a device architecture of photoconductors or transistors.[29–36] Unfortunately, these Sn-based PDs exhibit unsatisfactory response times, where FASnI$_3$-based PDs have delivered a rise/fall response time of 8.7/50 s and BA$_2$FASn$_2$I$_7$-based PDs showed a rise/fall response time of 5.78/0.96 s.[27,36] Recently, Seong and co-workers reported PDs based on 2D PEA$_2$SnI$_4$ with a fast response speed of 0.56 ms, but the associated wavelength range was limited to 300–650 nm.[37] In order to achieve faster response times, devices with short charge transport channels are needed, such as a vertical photodiode with a transparent electrode on one side.[38,39] However, there are only a few reports of Sn-based photodiodes, and even fewer dealing with 3D Sn-based PDs.[29,30,40,41] This is mainly due to the challenge of fabricating high quality and dense Sn-based perovskite thin films. Moreover, Sn-based perovskite thin films undergo Sn^{2+} oxidation to Sn^{4+} and rapid crystallization,[42–45] making it critical to achieve high quality and dense active films with low defect density to realize Sn-based perovskite PDs. Additive engineering to passivate defects and suppress Sn^{2+} oxidation is an effective way to obtain high quality Sn-based perovskite films.[46]

In this study, we have fabricated Pb-free perovskite PDs using a PEA$_{0.2}$FA$_{0.8}$SnI$_3$ thin film that incorporated 2-

*a*Key Laboratory of Photovoltaic Materials, Henan University, Kaifeng, Henan 475004, China. E-mail: liumy@vip.henu.edu.cn

*b*Institute of Molecular Plus and Tianjin Key Laboratory of Molecular Optoelectronic Science, Tianjin University, Tianjin 300072, China. E-mail: yaoxiang@tju.edu.cn

*c*Department of Materials Science and Engineering, City University of Hong Kong, Tat Chee Avenue, Kowloon, Hong Kong

*d*School of Energy and Environment, City University of Hong Kong, Tat Chee Avenue, Kowloon, Hong Kong

*e*Hong Kong Institute for Clean Energy, City University of Hong Kong, Tat Chee Avenue, Kowloon, Hong Kong. E-mail: a.yip@cityu.edu.hk

† Electronic supplementary information (ESI) available. See DOI: https://doi.org/10.1039/d3ta07499d

aminopyrimidine. The addition of 2-aminopyrimidine enabled controlled crystal growth, improved film morphology, passivated defect states, and prevented Sn^{2+} oxidation. The Sn-based PDs with 2-aminopyrimidine have exhibited a broad response range from 300 to 900 nm, a fast rise/fall response time of 0.93/1.74 ms, a high responsivity of 0.4 A W^{-1} and a detectivity of 1.16×10^{12} Jones, and a linear dynamic range (LDR) of 94.6 dB. Moreover, the $PEA_{0.2}FA_{0.8}SnI_3$-based PDs with 2-aminopyrimidine exhibited excellent operational stability after 10^4 on/off cycles.

Results and discussion

Sn-based perovskite films were prepared by the antisolvent-assisted spin-coating of a $PEA_{0.2}FA_{0.8}SnI_3$ precursor solution with varying amounts of 2-aminopyrimidine dissolved in a mixture of N,N-dimethylformamide (DMF) and dimethyl sulfoxide (DMSO) solvents, following the methodology outlined in the Experimental section. The impact of 2-aminopyrimidine concentration on the crystallinity and optical properties of $PEA_{0.2}FA_{0.8}SnI_3$ films was evaluated using X-ray diffraction (XRD) and absorption spectroscopy. The amount of 2-aminopyrimidine was adjusted from 0 to 2 mg to investigate the impact on the optoelectronic properties of $PEA_{0.2}FA_{0.8}SnI_3$ films. The XRD patterns, shown in Fig. 1a, are consistent with the reported orthorhombic structure of the perovskite film, with peaks at 14.1°, 24.5°, 28.4°and 43.0° attributed to the (100), (102), (200) and (213) planes, respectively.[47] The peaks located at

24.5° and 43.0° are too weak to be visible, and the enlarged patterns are shown in Fig. S1.† Increasing the amount of 2-aminopyrimidine (0–1 mg) led to an increase in the intensity of the (100) and (200) peaks indicating that the addition of 2-aminopyrimidine could regulate the crystalline process of the $PEA_{0.2}FA_{0.8}SnI_3$ films. However, the intensity of the (100) plane decreased when the $PEA_{0.2}FA_{0.8}SnI_3$ film was accompanied by 2 mg of 2-aminopyrimidine, suggesting that an excessive amount of additive hampers the growth of high-quality crystals in the $PEA_{0.2}FA_{0.8}SnI_3$ film. The full width at half maximum (FWHM) of the (100) diffraction peak is presented as a function of 2-aminopyrimidine concentration in Fig. 1b. As the amount of 2-aminopyrimidine additive increased from 0 to 1.0 mg, the FWHM of the (100) peak decreased from 0.0824° to 0.0807°. However, it increased to 0.089° with the addition of 2 mg. The $PEA_{0.2}FA_{0.8}SnI_3$ films treated with 1 mg 2-aminopyrimidine exhibited the smallest FWHM, indicating that the well-growth and high crystallinity of the $PEA_{0.2}FA_{0.8}SnI_3$ film could be attributed to the optimized amount of 2-aminopyrimidine.

The absorption spectra of the $PEA_{0.2}FA_{0.8}SnI_3$ films with varying 2-aminopyrimidine concentrations are presented in Fig. 1c. All the films exhibited an absorption edge at approximately 900 nm, which remained unaffected by the increasing amount of 2-aminopyrimidine (inset of Fig. 1c). This suggests that the additive had no significant effect on the absorption properties of the film. Steady-state photoluminescence (PL) measurements were performed to evaluate the optical properties of the $PEA_{0.2}FA_{0.8}SnI_3$ films as a function of 2-

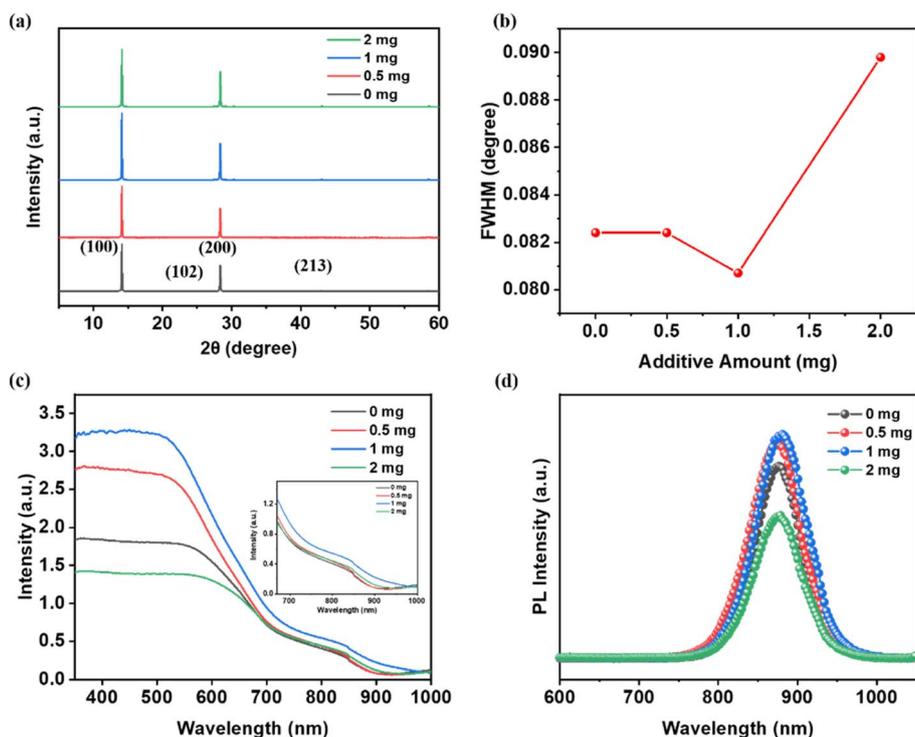**Fig. 1** (a) XRD diffraction patterns and (b) the FWHM of the (100) peak for $PEA_{0.2}FA_{0.8}SnI_3$ films with varying amounts of 2-aminopyrimidine (0–2 mg). (c) Absorption spectra (the inset shows the enlarged absorption edge) and (d) PL spectra of $PEA_{0.2}FA_{0.8}SnI_3$ films with varying amounts of 2-aminopyrimidine.

This journal is © The Royal Society of Chemistry 2024

J. Mater. Chem. A, 2024, **12**, 6446–6454 | **6447**

aminopyrimidine concentration. As shown in Fig. 1d, the films exhibited an emission peak at approximately 880 nm. The $PEA_{0.2}FA_{0.8}SnI_3$ film with 1 mg 2-aminopyrimidine exhibited the highest PL intensity, suggesting that the additive effectively passivated defect states and reduced non-radiative recombination losses.

To investigate the effect of the amounts of 2-amino-pyrimidine on the surface morphology and roughness of $PEA_{0.2}FA_{0.8}SnI_3$ films, we employed scanning electron microscopy (SEM) and atomic force microscopy (AFM). In Fig. 2a, the $PEA_{0.2}FA_{0.8}SnI_3$ film without 2-aminopyrimidine showed poor uniformity and numerous cracks, which can act as charge recombination centers and are detrimental to dark current. Furthermore, the pristine film exhibited a rough surface with a high roughness value of 31 nm (Fig. S2†). However, as the amount of 2-aminopyrimidine was increased from 0 to 1 mg (Fig. 2b and c), the film became denser and smoother. A more uniform morphology is crucial for efficient charge transport during photodetection. Additionally, the $PEA_{0.2}FA_{0.8}SnI_3$ film with 1 mg 2-aminopyrimidine displayed the lowest roughness value (13.2 nm). On the other hand, increasing the additive to 2 mg resulted in the appearance of numerous pinholes at the grain boundaries, leading to an increase in the roughness value (32 nm) (Fig. 2d and S2†). These results indicate that the use of excessive additives has a negative effect on the crystallization and leads to poor surface coverage. Therefore, adding 1 mg of 2-aminopyrimidine was found to be optimal, and the subsequent discussion will focus on the $PEA_{0.2}FA_{0.8}SnI_3$ film with 1 mg 2-aminopyrimidine and the pristine $PEA_{0.2}FA_{0.8}SnI_3$ film.

To explore the chemical interaction between the 2-amino-pyrimidine additive and the $PEA_{0.2}FA_{0.8}SnI_3$ film, Fourier transform infrared (FTIR) spectroscopy was conducted. As shown in Fig. S3,† the FTIR spectra of neat 2-aminopyrimidine and the perovskite with 1 mg of 2-aminopyrimidine were

compared. In neat 2-aminopyrimidine, the peak corresponding to the N–H bond in 2-aminopyrimidine was observed at 3400.2 cm^{-1}. However, in the perovskite with 2-amino-pyrimidine, the peak corresponding to the N–H bond shifted to 3384.9 cm^{-1}, indicating an interaction between 2-amino-pyrimidine and the perovskite. Furthermore, X-ray photoelectron spectroscopy (XPS) measurements were performed to examine the valence state of Sn and to assess the effect of the additive on the stability of the Sn-based perovskite. The Sn 3d core-level XPS spectra of the $PEA_{0.2}FA_{0.8}SnI_3$ films without and with 2-aminopyrimidine are presented in Fig. 3a and b, respectively. The peaks at 486.1 and 494.6 eV correspond to the energy levels of Sn $3d_{5/2}$ and $3d_{3/2}$ for Sn^{2+}, while the peaks at 486.8 and 495.0 eV correspond to Sn^{4+}.[48] Fitting analysis has revealed that the peak composition associated with Sn^{4+} decreased from 36.2 to 26.1% area following the introduction of 2-aminopyrimidine, indicating an effective inhibition of Sn^{2+} oxidation. Therefore, the introduction of the 2-amino-pyrimidine additive can significantly enhance film quality through the N–H bond and improve stability by suppressing the oxidation of Sn^{2+} to Sn^{4+}.

To validate the possible effect of 2-aminopyrimidine in reducing trap densities in $PEA_{0.2}FA_{0.8}SnI_3$ films, we fabricated electron-only devices with the structure of ITO/SnO$_2$/PEA$_{0.2}$FA$_{0.8}$-SnI$_3$/PCBM/Ag. The corresponding current–voltage curves are plotted in Fig. 3c and d using the space charge limited current (SCLC) method. The trap density (N_t) can be calculated using the equation, $N_t = 2\varepsilon_0\varepsilon_r V_{TFL}/eL^2$, where ε_r represents the relative dielectric constant, ε_0 is the vacuum permittivity, V_{TFL} denotes the trap-filled voltage, e is the elementary charge, and L is the thickness of the $PEA_{0.2}FA_{0.8}SnI_3$ layer.[49] The V_{TFL} value of $PEA_{0.2}FA_{0.8}$-SnI$_3$-based devices with and without 2-aminopyrimidine was 0.24 and 0.16 V, respectively. The incorporation of 2-aminopyrimidine resulted in a lower trap density (5.8×10^{15} cm^{-3}) compared to the

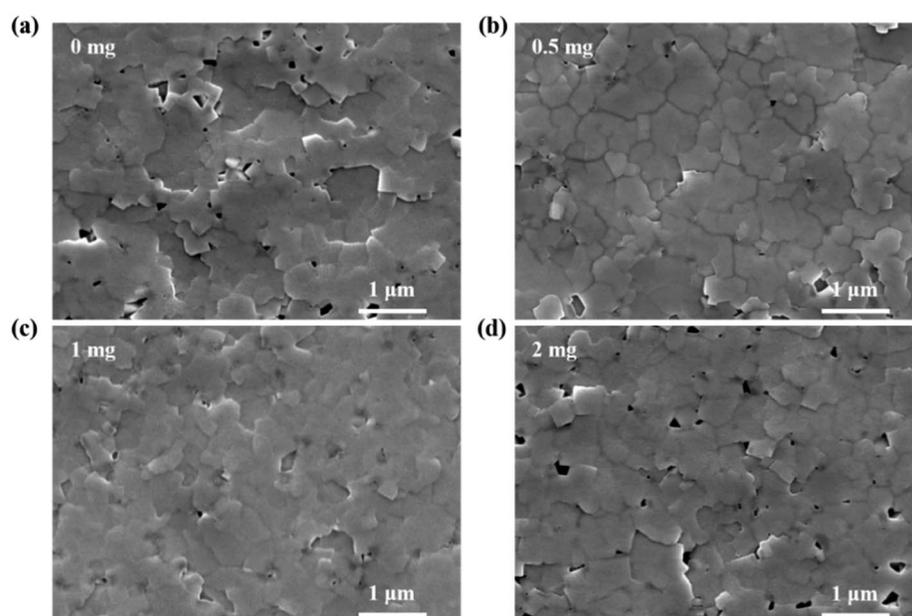Fig. 2 Representative SEM images of $PEA_{0.2}FA_{0.8}SnI_3$ films with (a) 0 mg, (b) 0.5 mg, (c) 1 mg and (d) 2 mg 2-aminopyrimidine.
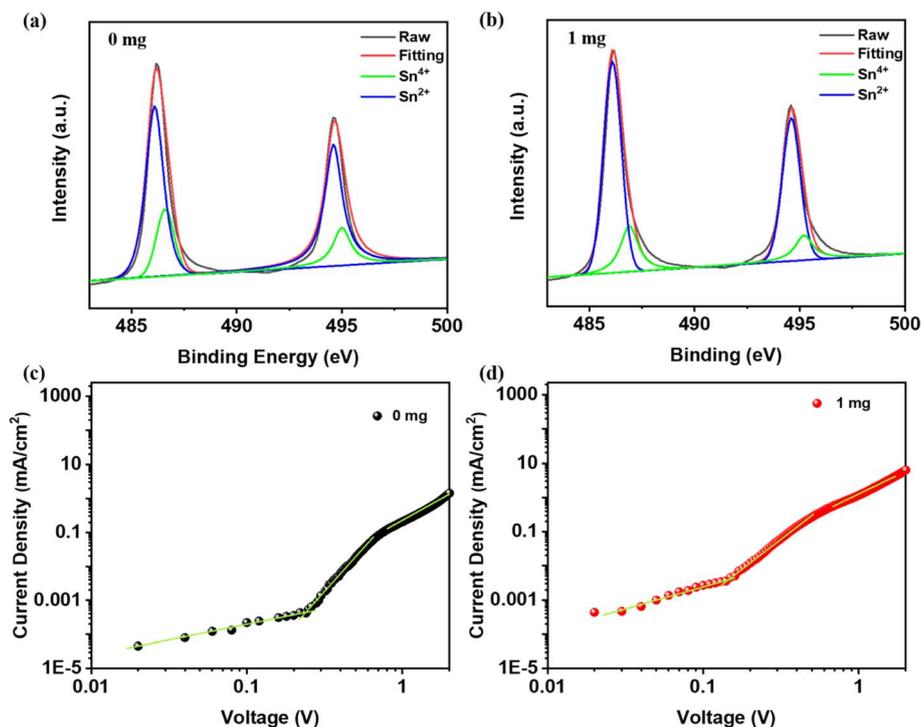
6448 | J. Mater. Chem. A, 2024, 12, 6446–6454

This journal is © The Royal Society of Chemistry 2024

Fig. 3 (a and b) XPS spectra, and (c and d) J–V curves for the electron-only devices based on the $PEA_{0.2}FA_{0.8}SnI_3$ films without and with 1 mg 2-aminopyrimidine.

film without 2-aminopyrimidine (3.9×10^{15} cm^{-3}), confirming that the additive can effectively reduce trap densities. This reduction in trap density can be attributed to the improved film quality and suppressed Sn^{2+} oxidation, leading to a decrease in dark current and an enhancement in PL intensity, which are beneficial features for high-performance photodetectors.

The schematic diagram in Fig. 4a illustrates the structural arrangement of the $PEA_{0.2}FA_{0.8}SnI_3$-based PDs. The PDs were fabricated with the structure of ITO/poly(3,4-ethylene dioxy-thiophene):polystyrene sulfonate (PEDOT:PSS)/$PEA_{0.2}FA_{0.8}SnI_3$/[6,6]-phenyl C_{61}-butyric acid methyl ester (PCBM)/Bathocuproine (BCP)/Ag. The effect of the 2-aminopyrimidine additive on the performance of the PDs was evaluated using current density–voltage (J–V) curves in the dark and under light illumination. The J–V curves of the $PEA_{0.2}FA_{0.8}SnI_3$-based perovskite PDs with and without 2-aminopyrimidine are shown in Fig. 4b. The current density of the $PEA_{0.2}FA_{0.8}SnI_3$-based PDs with 1 mg 2-aminopyrimidine was 3.69×10^{-7} A cm^{-2} at −0.1 V, lower than that of the PDs without 2-aminopyrimidine (4.6×10^{-6} A cm^{-2} at −0.1 V). The reduction in dark current can be attributed to the improved uniformity of the films and the lower trap densities resulting from the introduction of 2-amino-pyrimidine. The dense and smooth morphology with enhanced crystallinity led to an increase in the photocurrent density for the $PEA_{0.2}FA_{0.8}SnI_3$-based PDs containing 2-aminopyrimidine, establishing efficient carrier transport in the device.

The external quantum efficiency (EQE) spectra of PDs with varying concentrations of 2-aminopyrimidine were measured, where all PDs exhibited a broadband light response from 300 to 900 nm (Fig. S4†). Notably, the PD with 1 mg 2-amino-pyrimidine achieved a high EQE of over 60% at 400–810 nm (Fig. 4c), demonstrating high charge-carrier collection efficiency. Responsivity (R) is a key parameter for evaluating the performance of a PD, representing the response efficiency of the PD to the optical signal. The value of R can be calculated from the equation, $R = EQE \times e/h\nu$, where e represents the elementary charge, h is Planck's constant, and ν denotes the frequency of the optical signal.[50] The dependence of responsivity on wavelength at zero voltage is presented in Fig. 4d. The $PEA_{0.2}FA_{0.8}SnI_3$-based PD with 1 mg 2-aminopyrimidine generated higher R values over the 300–900 nm range. The maximum R value was 0.4 A W^{-1} at 810 nm, demonstrating the suitability of the $PEA_{0.2}FA_{0.8}SnI_3$-based PDs for broadband detection from visible to NIR. The enhanced photoresponse performance of the $PEA_{0.2}FA_{0.8}SnI_3$-based PDs incorporating 1 mg of 2-amino-pyrimidine was superior to that of the PDs without 2-amino-pyrimidine (Table 1).

The specific detectivity (D^*) is a figure of merit used to quantify the capability of a photodetector to measure weak optical signals. The D^* can be calculated using the formula, $D^* = R/(2q_eJ_d)^{1/2}$, where J_d represents the dark current density. The detectivity profiles with respect to spectral wavelength are shown in Fig. 4e. The D^* values for the $PEA_{0.2}FA_{0.8}SnI_3$-based PDs with 1 mg of 2-aminopyrimidine were appreciably higher, with a maximum detectivity of 1.16×10^{12} Jones at 810 nm under a bias voltage of −0.1 V, four times higher than that of the pristine $PEA_{0.2}FA_{0.8}SnI_3$-based PDs (2.9×10^{11} Jones). The results indicate that the lower trap density, which suppressed carrier recombination, resulted in

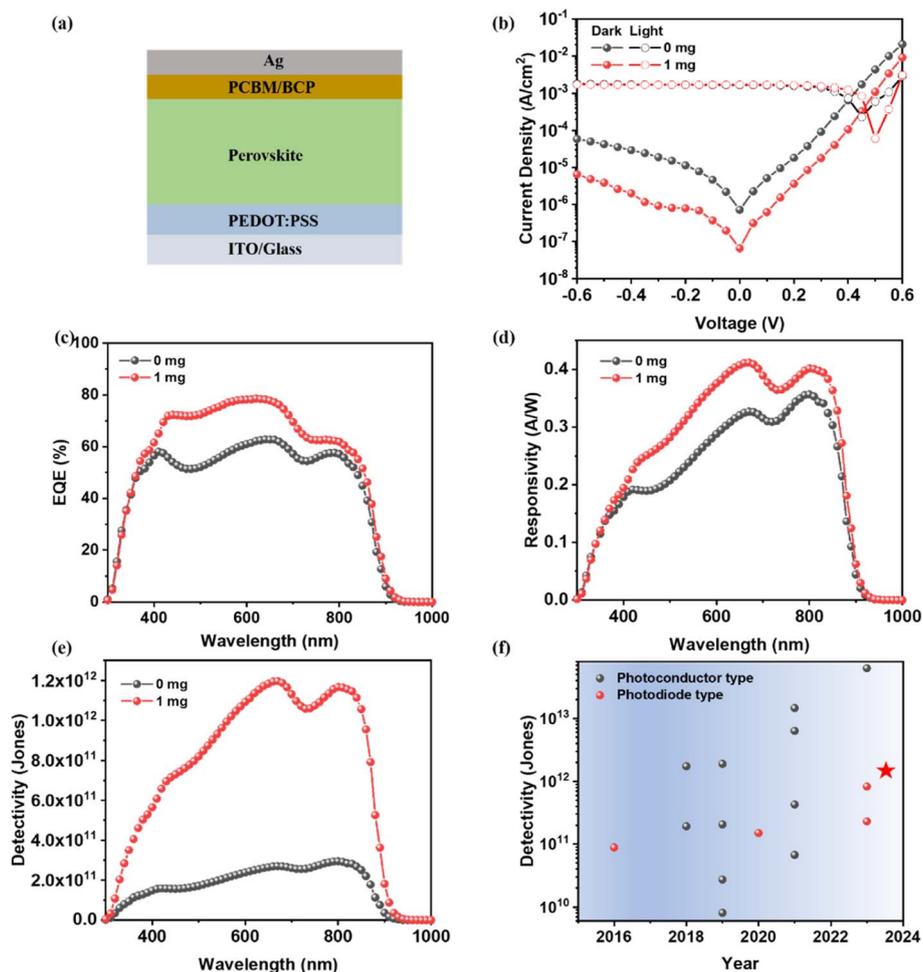This journal is © The Royal Society of Chemistry 2024

J. Mater. Chem. A, 2024, 12, 6446–6454 | 6449

Fig. 4 (a) Structure schematic of the Sn perovskite PDs. (b) $J-V$ curves under dark conditions and AM 1.5G solar illumination, (c) EQE spectra, (d) responsivity, and (e) specific detectivity of the Sn perovskite PDs with 0 mg (black circles) and 1 mg (red circles) 2-aminopyrimidine. (f) Representation of the specific detectivity of Sn-based perovskite PDs.

Table 1 Photoresponse performance of the $PEA_{0.2}FA_{0.8}SnI_3$-based PDs with and without 2-aminopyrimidine

	J_d (A cm^{-2})	R (A W^{-1})	D^* (Jones)	$T_{rise/fall}$ (ms)	LDR (dB)
Control	4.60×10^{-6}	0.35	2.90×10^{11}	0.99/1.78	71.4
2-Aminopyrimidine	3.69×10^{-7}	0.40	1.16×10^{12}	0.93/1.74	94.6

the highest R and D^* associated with the PDs containing 1 mg 2-aminopyrimidine. The range of D^* values reported for Sn-based PDs with different structures and active layers is summarized in Fig. 4f and Table 2. Previously reported Sn-based perovskite PDs with high D^* mostly employed two-dimensional or all-inorganic perovskites as photoactive layers, which resulted in a narrow device detection range. It should be noted that our fabricated $PEA_{0.2}FA_{0.8}SnI_3$-based PDs delivered the highest D^* when compared with previously reported Sn-based PDs based on a photodiode device architecture.

The linear dynamic range (LDR) is a crucial parameter that characterizes the range of linear dependence on light intensity and is particularly significant in practical photodetection

applications, specifically in imaging. It can be quantified using the formula, LDR $= 20 \log(I_{max}/I_{min})$, where I_{max} represents the highest light intensity and I_{min} indicates the lowest light intensity within the linear range. As illustrated in Fig. 5a, the I_{min} of the $PEA_{0.2}FA_{0.8}SnI_3$-based PDs with 1 mg 2-aminopyrimidine is one order of magnitude lower than that of the reference PDs (Fig. 5b). Both the reference and Sn-based $PEA_{0.2}FA_{0.8}SnI_3$ PDs with 1 mg 2-aminopyrimidine exhibited comparable upper limits. The LDR of the $PEA_{0.2}FA_{0.8}SnI_3$-based PDs with 1 mg 2-aminopyrimidine was 94.6 dB, significantly larger than the LDR of the PD without 2-aminopyrimidine (71.4 dB). This finding demonstrates that the addition of 2-aminopyrimidine can promote more effective charge separation and collection,

6450 | J. Mater. Chem. A, 2024, 12, 6446–6454

This journal is © The Royal Society of Chemistry 2024

Table 2 Comparison of the critical parameters associated with reported Sn-based PDs

Materials	D^* (Jones)	R (A W^{-1})	Response time	Structure type	Ref.
FASnI$_3$	1.9×10^{12}	1.1×10^5 @ 0.5 V	8.7/57 s	Photoconductor	27
Cs$_2$SnBr$_6$	2.71×10^{10}		9.52/4.34 ms	Photoconductor	31
Cs$_2$SnI$_6$			100/100 ms	Photoconductor	32
(PEA)$_2$SnI$_4$	1.92×10^{11}	16	0.63/3.6 s	Photoconductor	33
BA$_2$SnI$_4$	1.46×10^{13}	2.65 @ 4 V	2.62/0.3 s	Photoconductor	34
BA$_2$FASn$_2$I$_7$	6.3×10^{12}	1.55 @ 4 V	5.78/0.96 s	Photoconductor	34
CsSnBr$_3$	4.27×10^{11}	0.0623 @ 3 V	50/51 ms	Photoconductor	35
(PEA)$_2$SnI$_4$	2.06×10^{11}	3.29×10^3	0.37/3.05 s	Photoconductor	36
PEA$_2$SnI$_4$	6.32×10^{13}	509	0.56/10.7 ms	Photoconductor	37
(PEA)$_2$SnI$_4$	8.09×10^9	0.121	34/38 ms	Photoconductor	42
MA$_{0.7}$FA$_{0.3}$SnBr$_3$	6.7×10^{10}		45/420 ms	Photoconductor	44
(PEA)$_2$SnI$_4$	1.74×10^{12}	14.57 @ 10 V	50 ms/1.5 s	Photo transistor	43
MASnI$_3$	8.8×10^{10}	0.47	1500/400 ms	Photodiode Nanowire array	29
CsSnI$_3$	1.5×10^{11}	0.257	0.35/1.6 ms	Photodiode	30
PEA$_{0.15}$FA$_{0.85}$SnI$_3$	8.29×10^{11}	0.39	0.78/1.31 μs	Photodiode	40
FA$_{0.8}$PEA$_{0.2}$SnI$_3$	2.3×10^{11}	0.262	27.7/20.4 μs	Photodiode	41
PEA$_{0.2}$FA$_{0.8}$SnI$_3$	1.16×10^{12}	0.4	0.93/1.74 ms	Photodiode	This work
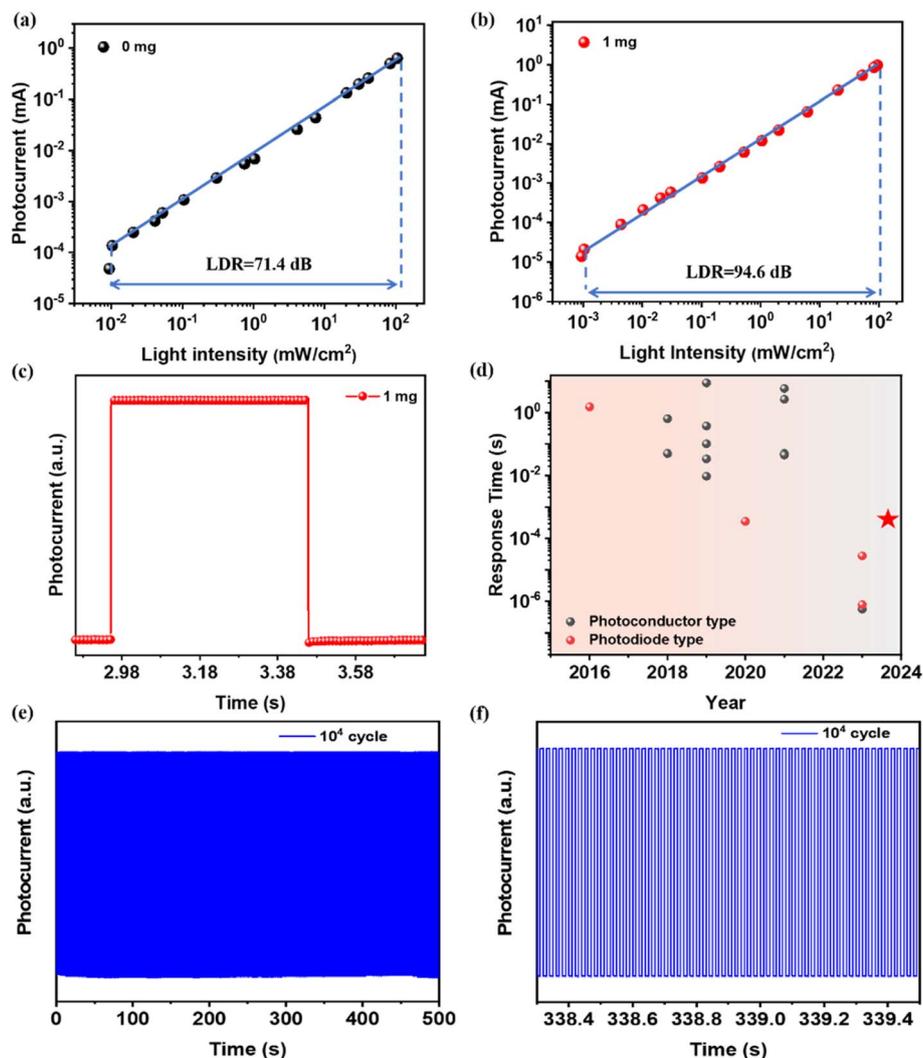
Fig. 5 (a and b) Photocurrent as a function of incident light intensity. (c) Response time of the PEA$_{0.2}$FA$_{0.8}$SnI$_3$-based PD with 1 mg 2-aminopyrimidine. (d) Response times of previously reported PEA$_{0.2}$FA$_{0.8}$SnI$_3$-based PDs. (e) Long-term I–t curve for the PEA$_{0.2}$FA$_{0.8}$SnI$_3$-based PD with 1 mg 2-aminopyrimidine under 533 nm green light illumination. (f) Enlarged I–t curve.

This journal is © The Royal Society of Chemistry 2024

J. Mater. Chem. A, 2024, **12**, 6446–6454 | **6451**

resulting in an enhanced response and detection over a wide range of light intensities, ranging from weak to intense.

The response time of $PEA_{0.2}FA_{0.8}SnI_3$-based PDs with 1 mg of 2-aminopyrimidine is shown in Fig. 5c, measured using an adjustable light source with current amplification. The rise and fall times were defined as the time required for the photocurrent to reach 10% and 90% of the maximum value, respectively. The PDs with 1 mg 2-aminopyrimidine exhibited a fast response speed, with a rise/fall time of 0.93/1.74 ms at 533 nm light illumination, appreciably faster than the pristine PDs (Fig. S5†). The fast response time of the PDs with 2-aminopyrimidine indicates that this additive effectively suppressed carrier recombination and minimized the dark current. Fig. 5d compares the response times of PDs using different Sn-based compounds, and it is evident that the PDs developed in this study showed a faster response time than other Sn-based perovskite PDs. Furthermore, when comparing response in terms of device structure (photodiode or photoconductor), our study delivers a similar response speed to the fastest response time Sn-based PDs reported previously. Additionally, the stability of the $PEA_{0.2}FA_{0.8}SnI_3$-based PDs with 1 mg 2-aminopyrimidine was superior to that of pristine PDs. Fig. 5 shows the device stability under green light with a pulse width of 50 Hz. The photocurrent did not exhibit any appreciable degradation after 10^4 on/off cycles, demonstrating excellent operation stability and repeatability. The stability was further illustrated by the enlarged I–t curve during testing in air that is presented in Fig. 5f. In contrast, the $PEA_{0.2}FA_{0.8}SnI_3$-based PD without 2-aminopyrimidine displayed noticeable degradation, as shown in Fig. S6,† indicating that the addition of 2-aminopyrimidine effectively improved the stability of Sn-based PDs.

Conclusions

In summary, we developed lead-free and environmentally friendly $PEA_{0.2}FA_{0.8}SnI_3$-based PDs by incorporating 2-aminopyrimidine as an additive. The addition of 2-aminopyrimidine not only regulated crystal quality, improved surface morphology, and decreased roughness of the $PEA_{0.2}FA_{0.8}SnI_3$ thin film, but also suppressed oxidation of Sn^{2+} and passivated defects. As a direct consequence, devices based on PDs with the 2-aminopyrimidine additive exhibited a lower defect density and dark current. The $PEA_{0.2}FA_{0.8}SnI_3$-based PDs achieved a high responsivity (0.4 A W^{-1}) and detectivity (1.16 × 10^{12} Jones) and fast response speed (0.93 ms). Additionally, the unencapsulated PDs exhibited excellent operation stability and repeatability after 10^4 on/off cycles. Our study demonstrates that the use of 2-aminopyrimidine as an additive is an effective means of producing high-performance Sn-based perovskite PDs.

Experimental section

Materials

Tin iodide (SnI_2, 99.999%), tin fluoride (SnF_2, 99.8%), dimethyl sulfoxide (DMSO, 99.8%), N,N-dimethylformamide (DMF, 99.8%), chlorobenzene (CB, 99.8%), and bathocuproine (BCP, 99.5%) were purchased from Sigma-Aldrich. Phenyl-ethylammonium iodide (PEAI, 99.5%) and formamidinium iodide (FAI, 99.5%) were purchased from Xi'an P-OLED Co. All materials and reagents were used as received without further purification.

Fabrication of perovskite photodetectors

The glass substrate with ITO was ultrasonically cleaned using acetone, ethyl alcohol, and deionized water and then treated with UV-ozone. The PEDOT:PSS (Clevios P VP Al 4083) layer was spin-coated onto the substrates at 4000 rpm for 30 s, followed by thermal annealing at 150 °C for 15 min in air. The Sn-based perovskite precursors were prepared by dissolving FAI : PEAI : SnI_2 : SnF_2 with a molar ratio of 0.8 : 0.2 : 1 : 0.1 in a 1 mL solution of DMF and DMSO (4 : 1 volume). In the case of the perovskite films with additives, a known amount of 2-aminopyridine was added to the precursor solution. In the fabrication of the Sn-based perovskite film, the precursor solution was filtered using a 0.22 μm PTFE filter and subjected to spin-coating at 1000 rpm for 10 s and then at 5000 rpm for 30 s. The antisolvent (CB) was dripped for 12 s in a high speed step. Then, the film was annealed at 70 °C for 10 min. PCBM (20 mg mL^{-1} in CB) was spun on the perovskite film at 1000 rpm for 20 s, followed by BCP (0.5 mg mL^{-1} in isopropyl alcohol) which was spun at 3000 rpm for 30 s. Finally, 100 nm thick Ag electrodes were deposited by thermal evaporation under a pressure of 5 × 10^{-4} Pa.

Film characterization

SEM images were obtained using a JSM-7001F scanning electron microscope. Sample roughness was determined with a Bruker Multimode 8 instrument. XRD analysis was conducted using Cu Kα radiation (Bruker D8 Advance). UV-visible absorption spectroscopy was performed using a UH4150 spectrophotometer. The PL spectra were measured using a fluorescence spectrometer (PerkinElmer LS 55), and XPS spectra were collected using a K-ALPHA+ XPS.

Device characterization

Current density as a function of voltage was recorded using a Keithley 2400 instrument under dark conditions and simulated AM1.5G sunlight generated using a solar simulator (SS-F5-3A, Enli Technology Co., Ltd). The light intensity was calibrated using a certified reference silicon cell. EQE measurements were conducted with a QE tester (Enlitech, QE-R 3018). A linear dynamic range test was performed at different white light intensities using ThorLabs metallic-coated neutral density filters. The on/off PD response was measured using a galvanostatic instrument (Metrohm Autolab PGSTAT204) with a light emitting diode (Ocean Optics (LSM)) at a wavelength of 533 nm. The LED pulse was generated using an LED controller (Ocean Optics, LDC-1).

Conflicts of interest

The authors declare that they have no known competing financial interests or personal relationships that influenced the work reported in this paper.

6452 | J. Mater. Chem. A, 2024, **12**, 6446–6454

This journal is © The Royal Society of Chemistry 2024

Acknowledgements

References

1 F. Teng, K. Hu, W. Ouyang and X. Fang, *Adv. Mater.*, 2018, **30**, 1706262.

2 S. Chen, C. Teng, M. Zhang, Y. Li, D. Xie and G. Shi, *Adv. Mater.*, 2016, **28**, 5969–5974.

3 A. Armin, R. D. Jansen-van Vuuren, N. Kopidakis, P. L. Burn and P. Meredith, *Nat. Commun.*, 2015, **6**, 6343.

4 H. Chen, H. Liu, Z. Zhang, K. Hu and X. Fang, *Adv. Mater.*, 2016, **28**, 403–433.

5 F. P. García de Arquer, A. Armin, P. Meredith and E. H. Sargent, *Nat. Rev. Mater.*, 2017, **2**, 1.

6 P. C. Y. Chow and T. Someya, *Adv. Mater.*, 2020, **32**, 1902045.

7 H. Qiao, Z. Huang, X. Ren, S. Liu, Y. Zhang, X. Qi and H. Zhang, *Adv. Opt. Mater.*, 2020, **8**, 1900765.

8 C. Xie, C.-K. Liu, H.-L. Loi and F. Yan, *Adv. Funct. Mater.*, 2020, **30**, 1903907.

9 P. Bhatnagar, M. Patel, K. Lee and J. Kim, *InfoMat*, 2023, **5**, e12408.

10 Q. Jiang, J. Tong, R. A. Scheidt, X. Wang, A. E. Louks, Y. Xian, R. Tirawat, A. F. Palmstrom, M. P. Hautzinger, S. P. Harvey, S. Johnston, L. T. Schelhas, B. W. Larson, E. L. Warren, M. C. Beard, J. J. Berry, Y. Yan and K. Zhu, *Science*, 2022, **378**, 1295–1300.

11 C. Li, X. Wang, E. Bi, F. Jiang, S. M. Park, Y. Li, L. Chen, Z. Wang, L. Zeng, H. Chen, Y. Liu, C. R. Grice, A. Abudulimu, J. Chung, Y. Xian, T. Zhu, H. Lai, B. Chen, R. J. Ellingson, F. Fu, D. S. Ginger, Z. Song, E. H. Sargent and Y. Yan, *Science*, 2023, **379**, 690–694.

12 Y. Jiang, C. Sun, J. Xu, S. Li, M. Cui, X. Fu, Y. Liu, Y. Liu, H. Wan, K. Wei, T. Zhou, W. Zhang, Y. Yang, J. Yang, C. Qin, S. Gao, J. Pan, Y. Liu, S. Hoogland, E. H. Sargent, J. Chen and M. Yuan, *Nature*, 2022, **612**, 679–684.

13 Z. Chu, Q. Ye, Y. Zhao, F. Ma, Z. Yin, X. Zhang and J. You, *Adv. Mater.*, 2021, **33**, 2007169.

14 Y. Fang, Q. Dong, Y. Shao, Y. Yuan and J. Huang, *Nat. Photonics*, 2015, **9**, 679–686.

15 L. Li, H. Chen, Z. Fang, X. Meng, C. Zuo, M. Lv, Y. Tian, Y. Fang, Z. Xiao, C. Shan, Z. Xiao, Z. Jin, G. Shen, L. Shen and L. Ding, *Adv. Mater.*, 2020, **32**, 1907257.

16 C. Chen, Y. Zhu, D. Gao, M. Li, Z. Zhang, H. Chen, Y. Feng, C. Wang, J. Sun, J. Chen, H. Tian, L. Ding and C. Chen, *Small*, 2023, **19**, 2303200.

17 Y. Zhou, C. Fei, M. A. Uddin, L. Zhao, Z. Ni and J. Huang, *Nature*, 2023, **616**, 712–718.

18 H. Liu, H. L. Zhu, Z. Wang, X. Wu, Z. Huang, M. R. Huqe, J. A. Zapien, X. Lu and W. C. H. Choy, *Adv. Funct. Mater.*, 2021, **31**, 2010532.

19 Y. Fang and J. Huang, *Adv. Mater.*, 2015, **27**, 2804–2810.

20 J. Wang, S. Xiao, W. Qian, K. Zhang, J. Yu, X. Xu, G. Wang, S. Zheng and S. Yang, *Adv. Mater.*, 2021, **33**, 2005557.

21 Q. Song, Y. Wang, F. Vogelbacher, Y. Zhan, D. Zhu, Y. Lan, W. Fang, Z. Zhang, L. Jiang, Y. Song and M. Li, *Adv. Energy Mater.*, 2021, **11**, 2100742.

22 A. Abate, *Joule*, 2017, **1**, 659.

23 X. Li, F. Zhang, H. He, J. J. Berry, K. Zhu and T. Xu, *Nature*, 2020, **578**, 555–558.

24 J. Cao and F. Yan, *Energy Environ. Sci.*, 2021, **14**, 1286–1325.

25 Y. Zhang, Y. Ma, Y. Wang, X. Zhang, C. Zuo, L. Shen and L. Ding, *Adv. Mater.*, 2021, **33**, 2006691.

26 M. M. Byranvand, W. Zuo, R. Imani, M. Pazoki and M. Saliba, *Chem. Sci.*, 2022, **13**, 6766–6781.

27 C.-K. Liu, Q. Tai, N. Wang, G. Tang, H.-L. Loi and F. Yan, *Adv. Sci.*, 2019, **6**, 1900751.

28 M. Han, J. Sun, M. Peng, N. Han, Z. Chen, D. Liu, Y. Guo, S. Zhao, C. Shan, T. Xu, X. Hao, W. Hu and Z. Yang, *J. Phys. Chem. C*, 2019, **123**, 17566–17573.

29 A. Waleed, M. M. Tavakoli, L. Gu, Z. Wang, D. Zhang, A. Manikandan, Q. Zhang, R. Zhang, Y.-L. Chueh and Z. Fan, *Nano Lett.*, 2017, **17**, 523–530.

30 F. Cao, W. Tian, M. Wang, M. Wang and L. Li, *InfoMat*, 2020, **2**, 577–584.

31 J. Zhou, J. Luo, X. Rong, P. Wei, M. S. Molokeev, Y. Huang, J. Zhao, Q. Liu, X. Zhang, J. Tang and Z. Xia, *Adv. Opt. Mater.*, 2019, **7**, 1900139.

32 X. Han, J. Liang, J.-H. Yang, K. Soni, Q. Fang, W. Wang, J. Zhang, S. Jia, A. A. Martí, Y. Zhao and J. Lou, *Small*, 2019, **15**, 1901650.

33 L. Qian, Y. Sun, M. Wu, C. Li, D. Xie, L. Ding and G. Shi, *Nanoscale*, 2018, **10**, 6837–6843.

34 Y. Yang, H. Zhang, S. Hou, T. Wang, W. Chen, S. Xian, Z. Zhang and Y. Mao, *Appl. Phys. Lett.*, 2021, **119**, 161106.

35 X. Ma, Y. Xu, S. Li, T. W. Lo, B. Zhang, A. L. Rogach and D. Lei, *Nano Lett.*, 2021, **21**, 9195–9202.

36 L. Qian, Y. Sun, M. Sun, Z. Fang, L. Li, D. Xie, C. Li and L. Ding, *J. Mater. Chem. C*, 2019, **7**, 5353–5358.

37 K.-R. Yun, T.-J. Lee, S.-K. Kim, J.-H. Kim and T.-Y. Seong, *Adv. Opt. Mater.*, 2023, **11**, 2201974.

38 M. Ahmadi, T. Wu and B. Hu, *Adv. Mater.*, 2017, **29**, 1605242.

39 W. Jang, B. G. Kim, S. Seo, A. Shawky, M. S. Kim, K. Kim, B. Mikladal, E. I. Kauppinen, S. Maruyama and I. Jeon, *Nano Today*, 2021, **37**, 101081.

40 W. Jang, K. Kim, B. G. Kim, J.-S. Nam, I. Jeon and D. H. Wang, *Adv. Funct. Mater.*, 2022, **32**, 2207713.

41 M. He, Z. Xu, C. Zhao, Y. Gao, K. Ke, N. Liu, X. Yao, F. Kang, Y. Shen, L. Lin and G. Wei, *Adv. Funct. Mater.*, 2023, **33**, 2300282.

42 C. Fang, H. Wang, Z. Shen, H. Shen, S. Wang, J. Ma, J. Wang, H. Luo and D. Li, *ACS Appl. Mater. Interfaces*, 2019, **11**, 8419–8427.

43 H. Wang, Y. Chen, E. Lim, X. Wang, S. Yuan, X. Zhang, H. Lu, J. Wang, G. Wu, T. Lin, S. Sun, J. Wang, Y. Zhan, H. Shen, X. Meng and J. Chu, *J. Mater. Chem. C*, 2018, **6**, 12714–12720.

44 Y. Zhu, G. Lai, J. Yi, T. Zhang, Y. Zhang, S. Wen and H. Zhou, *J. Alloys Compd.*, 2021, **866**, 158990.

This journal is © The Royal Society of Chemistry 2024

J. Mater. Chem. A, 2024, **12**, 6446–6454 | **6453**

45 J. Liu, H. Yao, S. Wang, C. Wu, L. Ding and F. Hao, *Adv. Energy Mater.*, 2023, **13**, 2300696.

46 H. Zhang, L. Pfeifer, S. M. Zakeeruddin, J. Chu and M. Grätzel, *Nat. Rev. Chem*, 2023, **7**, 632–652.

47 B.-B. Yu, Z. Chen, Y. Zhu, Y. Wang, B. Han, G. Chen, X. Zhang, Z. Du and Z. He, *Adv. Mater.*, 2021, **33**, 2102055.

48 T.-B. Song, T. Yokoyama, C. C. Stoumpos, J. Logsdon, D. H. Cao, M. R. Wasielewski, S. Aramaki and M. G. Kanatzidis, *J. Am. Chem. Soc.*, 2017, **139**, 836–842.

49 M. Liu, Z. Chen, Y. Yang, H.-L. Yip and Y. Cao, *J. Mater. Chem. A*, 2019, **7**, 17324–17333.

50 L. Dou, Y. Yang, J. You, Z. Hong, W.-H. Chang, G. Li and Y. Yang, *Nat. Commun.*, 2014, **5**, 5404.

6454 | *J. Mater. Chem. A*, 2024, **12**, 6446–6454

This journal is © The Royal Society of Chemistry 2024